Palaeogeography, Palaeoclimatology, Palaeoecology 485 (2017) 260–270

Contents lists available at ScienceDirect

Palaeogeography, Palaeoclimatology, Palaeoecology

journal homepage: www.elsevier.com/locate/palaeo

Productivity-climate coupling recorded in Pleistocene sediments off Prydz Bay (East Antarctica)

Li Wu [a,*], Rujian Wang [a,*], Wenshen Xiao [a], Shulan Ge [b], Zhihua Chen [b], Wout Krijgsman [c]

[a] State Key Laboratory of Marine Geology, Tongji University, Shanghai 200092, China
[b] First Institute of Oceanography, State Oceanic Administration, Qingdao 266061, China
[c] Department of Earth Sciences, Utrecht University, Budapestlaan 17, 3584 CD Utrecht, The Netherlands

ARTICLE INFO

Article history:
Received 4 February 2017
Received in revised form 10 June 2017
Accepted 15 June 2017
Available online 21 June 2017

Keywords:
Orbital scales
Age model
Nutrient supply
CO_2 cycling
Carbonate preservation

ABSTRACT

Export-production in the Southern Ocean is thought to be tightly correlated with atmospheric CO_2 fluctuations over geological times. Relevant studies are, however, mainly confined to the Atlantic and Pacific sectors of the Southern Ocean and often only cover the last glacial-interglacial cycle. Here, we present a sediment record retrieved off Prydz Bay (East Antarctica) spanning the last ~520 kyrs. We show that the distribution pattern of local export production is closely coupled with global climate change on orbital time scales. We propose that the dominant factors controlling local export production include the amount of nutrients supply from the ocean interior and the extent of sea ice cover, thus representing the combined history of deep water exposure/ventilation and the sea ice coverage in the studied area. Sharp increases in the local export production coincide with abrupt increase in atmospheric CO_2 concentrations during deglacial periods, indicating drastic outgassing of the upwelled deep water in the Southern Ocean. Gradually decrease in the export production following interglacial peaks concurs with decrease in deep water exposure/ventilation and increase in sea ice cover, explaining the early decline in atmospheric CO_2 over a glacial-interglacial cycle.

1. Introduction

Marine oxygen isotope (Lisiecki and Raymo, 2005) and Antarctic ice core deuterium (EPICA-Community-Members, 2004) records show that after the Mid-Pleistocene Transition (MPT), global climate evolution is asymmetric on the glacial-interglacial time scale, with abrupt warming and gradual cooling. This saw-tooth pattern in temperature is tightly coupled with similar variations in atmospheric CO_2 concentration for at least the past ~800 kyrs (EPICA-Community-Members, 2004; Luthi et al., 2008). No single mechanism can fully account for the observed coupling (Archer et al., 2000; Sigman and Boyle, 2000). However, there is a general consensus that the ocean interior is a major agent modulating atmospheric CO_2 concentration (Adkins et al., 2002; Watson and Garabato, 2006; Toggweiler et al., 2006; Sigman and Boyle, 2000; Sikes, 2012) because the ocean interior contains 90% of the combined oceanic, atmospheric, and terrestrial carbon, and a rearrangement of deep water masses will thus have a large impact on the atmospheric carbon budget (Ferrari et al., 2014).

The Southern Ocean (SO) is considered to be the major interface of oceanic-atmospheric CO_2 exchange as it comprises the upwelling branch of meridional overturning circulation (MOC) (Marshall and Speer, 2012; Sigman et al., 2010; Jaccard et al., 2013). In the SO, a series of biological, chemical and physical mechanisms are involved in the CO_2 cycling process and play an important role in modulating global climate change (e.g., Elderfield and Rickaby, 2000; Frank et al., 2000; Moore et al., 2000; Sigman and Boyle, 2000; Stephens and Keeling, 2000; Schneider-Mor et al., 2005; Abelmann et al., 2006; Jaccard and Galbraith, 2012; Ferrari et al., 2014). Specifically, the 'biological pump' is a key mechanism to extract CO_2 from the atmosphere into the ocean interior (Jaccard et al., 2005; Sigman et al., 2010; Jaccard et al., 2013), and export production in the SO is thus an important parameter affecting global climate.

There are two modes of export production changes in the SO (Jaccard et al., 2013). They commonly co-vary with climate change, showing seesaw-like temporal patterns across the Antarctic Polar Front (APF) (Jaccard et al., 2013). In areas north of the APF, export production increases during cold periods and decreases during warm periods along with fluctuation in the dust input (e.g., Kumar et al., 1995; Anderson et al., 1998; Jaccard et al., 2013; Anderson et al., 2014; Lamy et al., 2014; Martínez-García et al., 2014; Manoj and Thamban, 2015). In contrast, south of the APF, export production decreases in cold intervals and increases in warm intervals, coinciding with variations of Antarctic atmospheric temperature and/or marine oxygen isotopes (e.g., Frank et al., 1995; Anderson et al., 1998; Bonn et al., 1998; Anderson et al., 2009; Jaccard et al., 2013; Xiao et al., 2016). Therefore, the temporal structure of the past glacial-interglacial atmospheric CO_2

* Corresponding authors at: State Key Laboratory of Marine Geology, Tongji University, 1239 Siping Road, Shanghai 200092, China.
E-mail addresses: wuli@tongji.edu.cn (L. Wu), rjwang@tongji.edu.cn (R. Wang).

http://dx.doi.org/10.1016/j.palaeo.2017.06.018
0031-0182/

change was probably determined by a combination of these two modes of export production changes in the SO (Jaccard et al., 2013). However, the poor preservation of biogenic carbonate records and the general absence of precise time frames for marine high latitude sediments of the SO have so far confined paleo-export production studies to the Atlantic and Pacific sectors of the SO (e.g., Frank et al., 2000; Anderson et al., 2009; Presti et al., 2011; Jaccard et al., 2013; Studer et al., 2015). Moreover, these studies mostly covered sediment records of the last glacial-interglacial cycle, thus restricting our understanding of the role the SO plays in modulating the atmospheric CO_2 budget over previous climate cycles.

In the present study, we investigate sediment records in three cores retrieved off Prydz Bay (East Antarctica) dating back to ~520 ka. X-Ray Fluorescence (XRF) geochemical element scanning, color reflectance and biogenic silica (opal) measurements, foraminifera abundance counting and AMS ^{14}C dating were conducted to 1) investigate temporal variations of the local export production; 2) establish a precise stratigraphic framework for these sediment cores; 3) explore the factors controlling the local export production; and 4) discuss the potential coupling between the local export production and atmospheric CO_2.

2. Regional setting

Prydz Bay is the third largest embayment around Antarctica with a surface area of about 80,000 km^2 (Taylor and McMinn, 2002). It is situated between 65°E and 80°E on the continental margin of Antarctica facing the Southern Indian Ocean (Fig. 1). The bay is located at the seaward terminus of a major Mesozoic graben structure, the Lambert Graben, which is now occupied by the Lambert Glacier and the Amery Ice Shelf (LG-AIS) (Passchier et al., 2003). The LG-AIS system is the largest outlet glacier system on Antarctica, draining 16–20% of the East Antarctic ice into the SO (Hannah, 2006).

The ocean current system around Prydz Bay is composed of five branches (Vaz and Lennon, 1996; Bindoff et al., 2000; Cooper and O'Brien, 2004) (Fig. 1). The Antarctic Coastal Current (CoC) flows westward, bringing in cold waters from the east. The Antarctic Slope Current (ASC) flows from east to west over the continental slope. Between the CoC and the ASC, the clockwise rotating Prydz Gyre mainly flows over the continental shelf. North of the ASC, the cyclonic Antarctic Divergence Zone (ADZ) intrudes into the shelf and brings up the relatively warm and salty Antarctic Deep Water (Yabuki et al., 2006). Further offshore, the northern Antarctic Circumpolar Current (ACC) flows eastward and connect the SO with other oceans.

Modern summer sea ice distribution is confined to the inner Prydz Bay, while modern winter sea ice can expand to the midline between the modern APF and the Prydz coastline (~58°S). During the Last Glacial Maximum (LGM), the winter sea ice limit had advanced to the position of modern APF (~51°S), while the summer sea ice limit was considered to be proximal to its modern position (Crosta et al., 1998a, b, 2004; Gersonde et al., 2005; Röthlisberger et al., 2010), or had even expanded to the modern winter sea ice limit (Goosse et al., 2013).

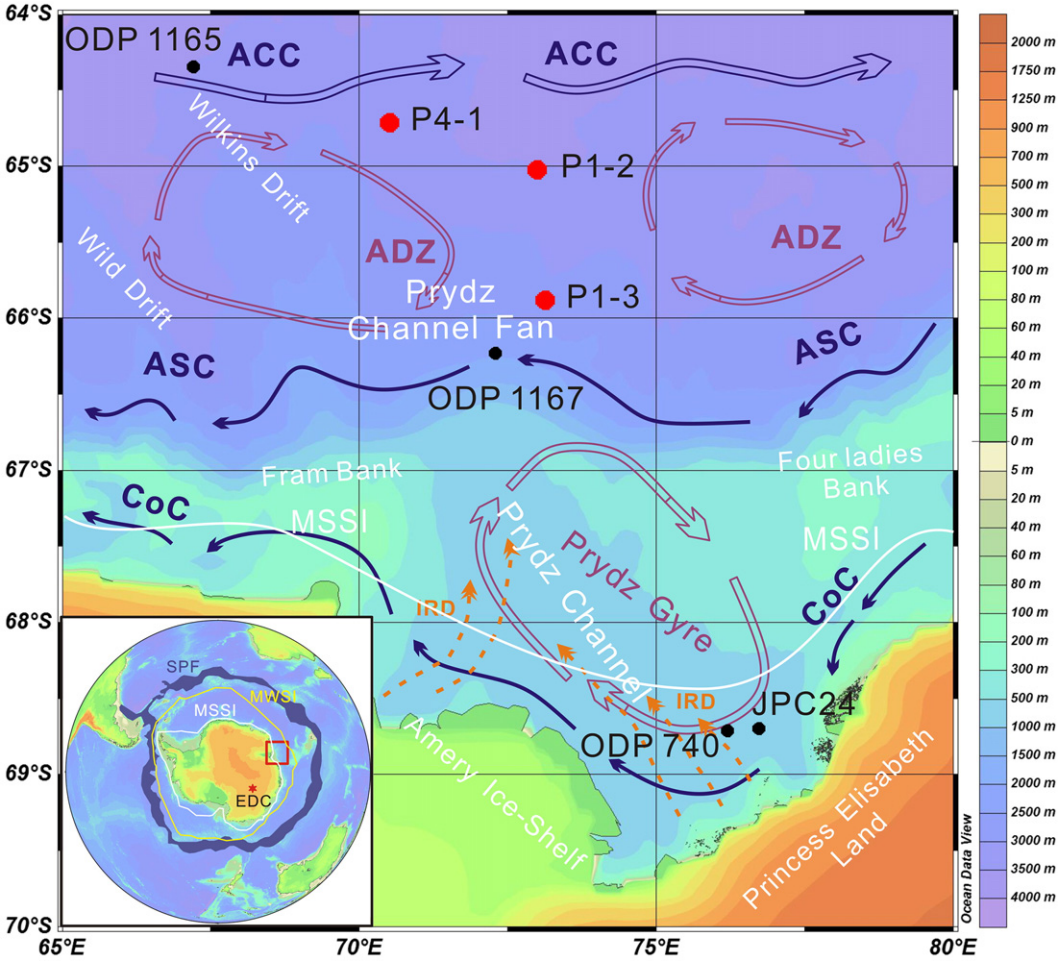

Fig. 1. Core sites and environmental setting of the Prydz Bay, East Antarctica. IRD: tracks of Ice Rafted Detritus. CoC: Antarctic Coastal Current. ASC: Antarctic Slope Current. ADZ; Antarctic Divergence Zone. ACC: Antarctic Circumpolar Current. IRD tracks and current system are based on Cooper and O'Brien (2004) and Forsberg et al. (2008). Core sites refer to Table 1. In the lower-left inset: EDC: EPICA Dome C ice core (EPICA-Community-Members, 2004). The deep blue shaded area denotes the modern Antarctic Polar Front zone (APF) modified after Röthlisberger et al. (2010). MWSI: Modern Winter Sea Ice edge. MSSI: Modern Summer Sea Ice edge. The Prydz Bay area is indicated by a red box.

The average sedimentation rate of the Pleistocene succession on the Prydz Bay slope and rise ranges from 0.69 to 1.22 cm/kyr according to the results of ODP Sites 1167 (Theissen et al., 2003) and 1165 (Junttila et al., 2005). Much higher sedimentation rates have been reported for the debris flow (diamicton) strata (~20 cm/kyr, Theissen et al., 2003) and the uppermost diatomaceous layer on the continental shelf (~100 cm/kyr) (e.g., Domack et al., 1991; Barbara et al., 2010).

In the Prydz Bay area, biogenic silica represents over 70% (by weight) of the particle flux to the deep ocean (Pilskaln et al., 2004). Biogenic silica and organic carbon contents both decrease with increasing water depth (Pilskaln et al., 2004), indicating significant opal dissolution and organic carbon remineralization during particle sinking.

3. Materials

Three gravity cores ANT29/P4-01 (P4-1), ANT30/P1-02 (P1-2) and ANT30/P1-03 (P1-3) were collected from the Prydz deep-sea region during the 29th and 30th Chinese Antarctica Expedition onboard R/V *Xuelong* to Prydz Bay in 2013 and 2014 (Table 1). The core sites are located far from submarine canyons thus sediments are not affected by turbidity or debris flows. The sediment color of the three cores varies from olive, brown to gray. According to wet and dry sieving experiments, the core sediments principally consist of clayey silt with a minor proportion of coarse grains (63 μm to 2 mm, ~6.2 wt%) and a few randomly distributed pebble (>2 mm) recognized as Ice Rafted Detritus (IRD).

4. Methods

4.1. Experimental procedures

Color reflectance was measured using a Minolta CM-2002 hand-held spectrophotometer on freshly split core halves in 1-cm increments. It provides quantitative measurements of the visible light spectrum from 400 to 700 nm, and automatically transfers the reflectance data into the CIE La*b* color space.

The distributions of elements on sample spots of 1 cm × 1 cm in size at 1-cm increments on split core surfaces were detected using an AVAATECH X-ray Fluorescence (XRF) Core Scanner. Each core segment was covered with a spex certiprep 3525 Ultralens foil (4 μm thick) to protect the probe of the scanner from contamination and was triple-scanned for elements from Al to Ba at 1 mA and different tube voltages (10 kv; 30 kv; 50 kv) with 30 s counting time.

Biogenic silica (opal) content of core P1-2 was determined on 0.15 g ground bulk sediment at 2-cm increments using the alkaline extraction method of Mortlock and Froelich (1989). Reproducibility measurements (n = 48) showed a relative standard deviation of <3%.

Foraminifera abundance of core P1-2 was determined under an optical microscope after successive wet and dry sieving the bulk sediments through 63 μm and 150 μm meshes, respectively. AMS ^{14}C dating was performed on shells of planktonic foraminifer *Neogloboquadrina pachyderma* (sin.) (Nps) (>150 μm size fraction) picked from core P1-2. The ^{14}C ages were calibrated to calendar ages using the Calib 7.0 program (Stuiver and Reimer, 1993) and a marine δ^{13}C radiocarbon age calibration curve (Reimer et al., 2013) with a carbon reservoir age of 1300 yr (Domack et al., 2001). Except AMS ^{14}C dating which was done at BETA Analytic Inc., Miami, other measurements were performed in the State Key Laboratory of Marine Geology, Tongji University.

Table 1
Information of sediment cores used in this study.

site	Abbr.	Longitude (°E)	Latitude (°S)	Water depth (m)	Length (cm)	Data source
ANT30/P1-03	P1-3	73.02	65.99	2542	599	Tang et al. (2016)
ANT30/P1-02	P1-2	72.94	65.01	2860	624	This study
ANT29/P4-01	P4-1	70.69	64.92	3162	421	This study

4.2. Excess silicon and barium calculations

Biogenic silica (bio-Si) and biogenic barium (bio-Ba) are widely used as proxies for sea surface export production (Bonn et al., 1998; Pondaven et al., 2000; Schenau et al., 2001; Paytan and Griffith, 2007; Presti et al., 2011). In this study, they are also expressed as excess silicon (Si_{xs}) and excess Barium (Ba_{xs}), which were calculated from XRF-derived element composition data. Although the XRF core scanning cannot quantify the element content, XRF scanning results from fine-grained sediments has been shown to be positively correlated with those from conventional (quantitative) XRF and mass spectrometric techniques (Jansen et al., 1998; Tjallingii et al., 2007; Weltje and Tjallingii, 2008) and thus can provide high-quality data sets for time series reconstruction and stratigraphic correlations (Jaccard et al., 2005, 2010, 2013; Tian et al., 2011).

The deep sea sediments in the cores off Prydz Bay are a mixture predominantly consisting of biogenic and terrigenous materials, hence the bulk Si and Ba can be expressed as:

$$Si = Si_{det} + Si_{xs} \quad (1)$$

$$Ba = Ba_{det} + Ba_{xs} \quad (2)$$

where Si_{det} and Ba_{det} are silicon and barium of terrigenous origin, while Si_{xs} and Ba_{xs} are those of biogenic excess, which thus can be determined by subtracting the Si_{det} and Ba_{det} from the bulk Si and Ba, respectively.

Generally, Si_{det} and Ba_{det} can be estimated using a normalization method assuming the Al content is proportional to the detrital component in the sediments (e.g., Bonn et al., 1998). However, this normalization method cannot be directly applied to this study as the elemental results here were semi-quantitatively determined. Thus we slightly modified this normalization method as detailed in the supplementary material. In practice, we normalized the resulting Si_{xs} and Ba_{xs} to emphasize their variances because only the distribution pattern of these export production proxies are used. The normalized Si_{xs} and Ba_{xs} are referred to as Si_{xsn} and Ba_{xsn} in the following text.

4.3. Age model and test procedures

We applied both manual tuning (Analyseries) (Paillard et al., 1996) and dynamic time warping algorithms (match) (Lisiecki and Lisiecki, 2002), which can compute a time axis stretching and map two time series optimally by minimizing their mutual covariance, to construct an optimal age model for our cores. Cross wavelet transform (XWT) (Grinsted et al., 2004) was used to test the matching levels.

5. Results

5.1. Down-core patterns of physical and chemical parameters

The digital images (Figs. 2, S1, S2) of the studied core surfaces using color reflectance data show relatively thick light-colored sediments were regularly interrupted by thin dark layers (e.g., 210 cm, 310 cm 390 cm and 530 cm in P1-2). Lighter intervals with high a* values generally correspond to high values of Si_{xsn}, Ba_{xsn} and opal, and vice versa for darker layers. The total Si curve is compatible to that of Al, indicating that most of Si was derived from terrigenous detritus. But the resemblance between Ba and Ba_{xsn} in all the three cores (Figs. 2, S1, S2) implies its predominant biogenic origin. Remarkably, the variations of biogenic Si_{xsn} and biogenic Ba_{xsn} for all the three cores are similar.

Opal content of P1-2 varies between 3.21 and 21.3 wt%, with an average of 9.70 wt% (Fig. 2). As the dominant biogenic component in

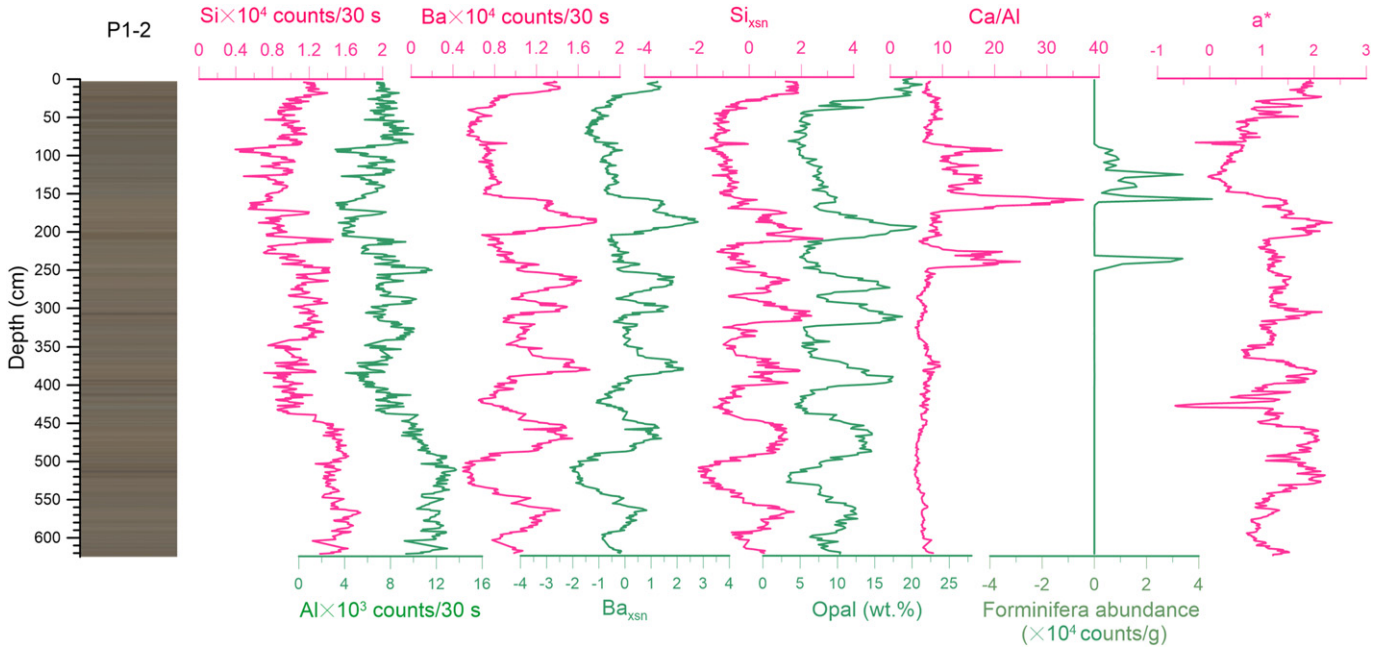

Fig. 2. Down core distribution patterns of XRF-derived Si, Al, Ba, Ba_{xsn}, Si_{xsn}, and Ca/Al ratio, opal content, foraminifera abundance and color a* of core P1-2.

the sediment, its down core pattern is generally consistent with that of Si_{xsn} ($r^2 = 0.701$), suggesting that opal can be used to represent Si_{xsn} variations in the cores.

Ca/Al ratios and foraminifera abundance both are proxies of biogenic carbonates. Their down-core patterns closely co-vary and show two intervals of relatively high values at the upper sections of the cores (Figs. 2, S1, S2), suggesting that the Ca/Al pattern can be used to represent biogenic carbonate over the studied interval.

5.2. AMS ^{14}C dating

AMS ^{14}C dating results of P1-2 (Table 2) show ages of 92–94 cm and 114–116 cm falling into early MIS 2 and late MIS 3, respectively. Deeper than 136 cm, the sediment is beyond the AMS ^{14}C dating limit.

6. Discussion

6.1. Export production variations

All proxies used to reconstruct past variability of export production are subject to potential biases, because the amount of biogenic material preserved in marine sediments is not only a function of the local export production, but also of the preservation efficiency in the sediments (Anderson et al., 2014). Quantifying preservation efficiency is, however, very difficult. An alternative to trace the temporal variation of export production is to use two export production proxies whose preservation efficiencies are independent of each other (Jaccard et al., 2010; Anderson et al., 2014). In this study, we use opal (Bio-Si or Si_{xsn}) and biogenic barium (Bio-Ba or Ba_{xsn}) to examine export production variations in cored sediments of the study area.

Temperature is considered to be an important control factor on opal preservation (Bidle et al., 2002). However, in the constantly cold environment of the abyssal ocean, opal preservation depends mainly on the accumulation rate (Pondaven et al., 2000; Sayles et al., 2001). The preservation of biogenic barium mainly depends on paleo-environmental conditions as $BaSO_4$ is dissolvable when sulphate-depleted/anoxic conditions prevail (McManus et al., 1998; Anderson et al., 2002; van Beek et al., 2003; Tribovillard et al., 2006). The preservation efficiencies of opal (Si_{xsn}) and biogenic barium in the SO are thus controlled by different factors, which should have been reflected in their distribution patterns if preservation efficiency had played a role. In the Prydz Bay cores, however, this is not the case, as both opal (Si_{xsn}) and biogenic barium show very similar distribution patterns (Figs. 2, S1, S2), suggesting that they are primarily controlled by export production.

Nevertheless, different preservation efficiencies could well have played a secondary role on the down-core patterns of these proxies. At some specific intervals, for example, Si_{xsn} increases leads Ba_{xsn} increases (e.g., ~25–50 cm, ~200–225 cm, ~300–325 cm, ~475–500 cm of core P1-2, ~25–50 cm, ~175–200 cm, ~275–300 cm of core P1-3 and ~125–150 cm, ~200–225 cm, ~275–300 cm of core P4-1), but Si_{xsn} decreases also leads Ba_{xsn} decreases at other intervals (e.g., ~150–175 cm in core P1-2, and ~80–110 cm in core P4-1) (Figs. 2, S1, S2). These observations appear to support that the preservation efficiency of bio-Si was best at relatively high bio-Si accumulation rates (Pondaven et al., 2000; Sayles et al., 2001). Meanwhile, a relatively high organic carbon flux would result in more reduction conditions and dissolution of bio-Ba in the sediment and/or at the sediment-water interface. The preservation of bio-Si would be diminished when bio-Si accumulation rates were low, but the preservation of bio-Ba would be better due to reduced organic carbon fluxes (McManus et al., 1998; Anderson et al., 2002; van Beek et al., 2003; Tribovillard et al., 2006). Therefore, neither Ba_{xsn} nor Si_{xsn} alone can fully reflect the temporal variation pattern of the local export production in our study area.

Table 2
AMS ^{14}C dating results on *Neogloboquadrina pachyderma* (sin.) from P1-2.

Sample code	Depth (cm)	AMS ^{14}C age (yr)	Reservoir corrected ^{14}C age (yr)	Calibrated age (yr BP)
BETA 395571	92–94	24,710 ± 110	23,410 ± 110	27,443 ± 223
BETA 400276	114–116	34,050 ± 240	32,750 ± 240	36,661 ± 355
BETA 400277	136–138	>43,500	–	–
BETA 395573	162–164	>43,500	–	–
BETA 395574	226–228	>43,500	–	–

Note: *A 1300 yr reservoir effect was applied according to (Domack et al., 2001). The ^{14}C ages were calibrated using Calib 7.0 program (Stuiver and Reimer, 1993) and Marine $\delta^{13}C$ calibration curve (Reimer et al., 2013).

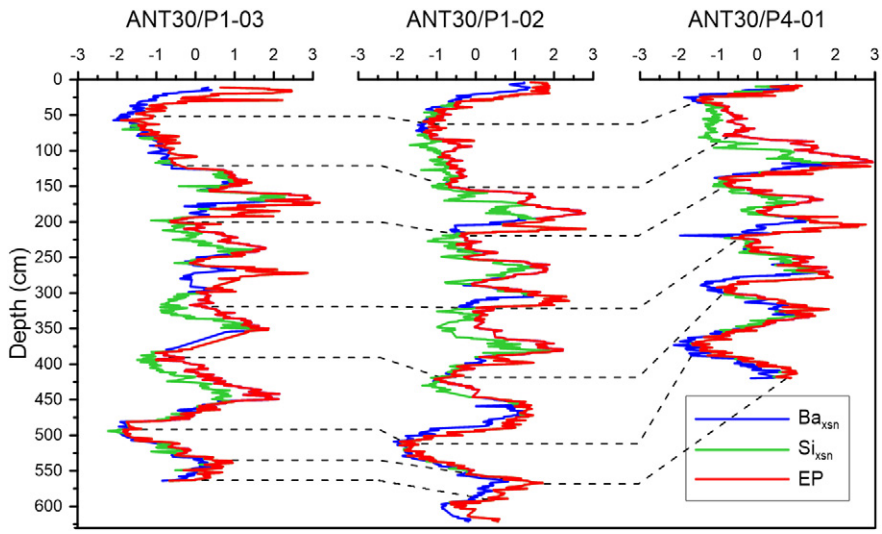

Fig. 3. Down-core distribution patterns of Si_{xsn}, Ba_{xsn} and EP of the three studied cores. EP can be used as a tool for regional stratigraphic correlation as indicated by the black dashed lines.

To circumvent these singular parameter deficiencies, we constructed a new series EP (Export production distributing Pattern) by calculating the maximal values of each pair of Si_{xsn} and Ba_{xsn} at the same depth of a core (Fig. 3). In practice, EP and Si_{xsn} will have similar down-core patterns at better bio-Si preservation intervals, and EP and Ba_{xsn} will be comparable when bio-Ba preservation was better (Fig. 3).

As shown in Fig. 3, the similar EP records for all the three cores enabled us to align the records of cores P1-03 and P4-01 to the longest record of core P1-2 using the match software (Lisiecki and Lisiecki, 2002). In turn, other records such as Si_{xsn}, Ba_{xsn}, a* and Ca/Al were also aligned simultaneously (Fig. 4). In addition, we constructed an EP stack by averaging the three aligned EP records (Fig. 5A) to enhance the signal-to-noise ratio. This EP stack is used here to represent the variations of local export production off Prydz Bay.

6.2. Age models based on EP-LR04-$\delta^{18}O$ correlation

Marine sediments from south of the APF are often poorly dated due to a lack of biogenic carbonates (Hillenbrand et al., 2003; Xiao et al., 2016). An alternative method to construct high-resolution time frames for the SO sediments is correlating its marine proxy records to well-dated climate curves, e.g., the magnetic susceptibility vs. ice core dust records (Pugh et al., 2009; Weber et al., 2012; Xiao et al., 2016), and the abundance of specific diatom species vs. Marine oxygen isotope records (Anderson et al., 2009).

Previous studies indicated that temporal variations of export production in areas south of the APF are consistent with global climate changes (e.g., Frank et al., 1995; Anderson et al., 1998; Bonn et al., 1998; Anderson et al., 2009; Presti et al., 2011; Jaccard et al., 2013; Studer et al., 2015;

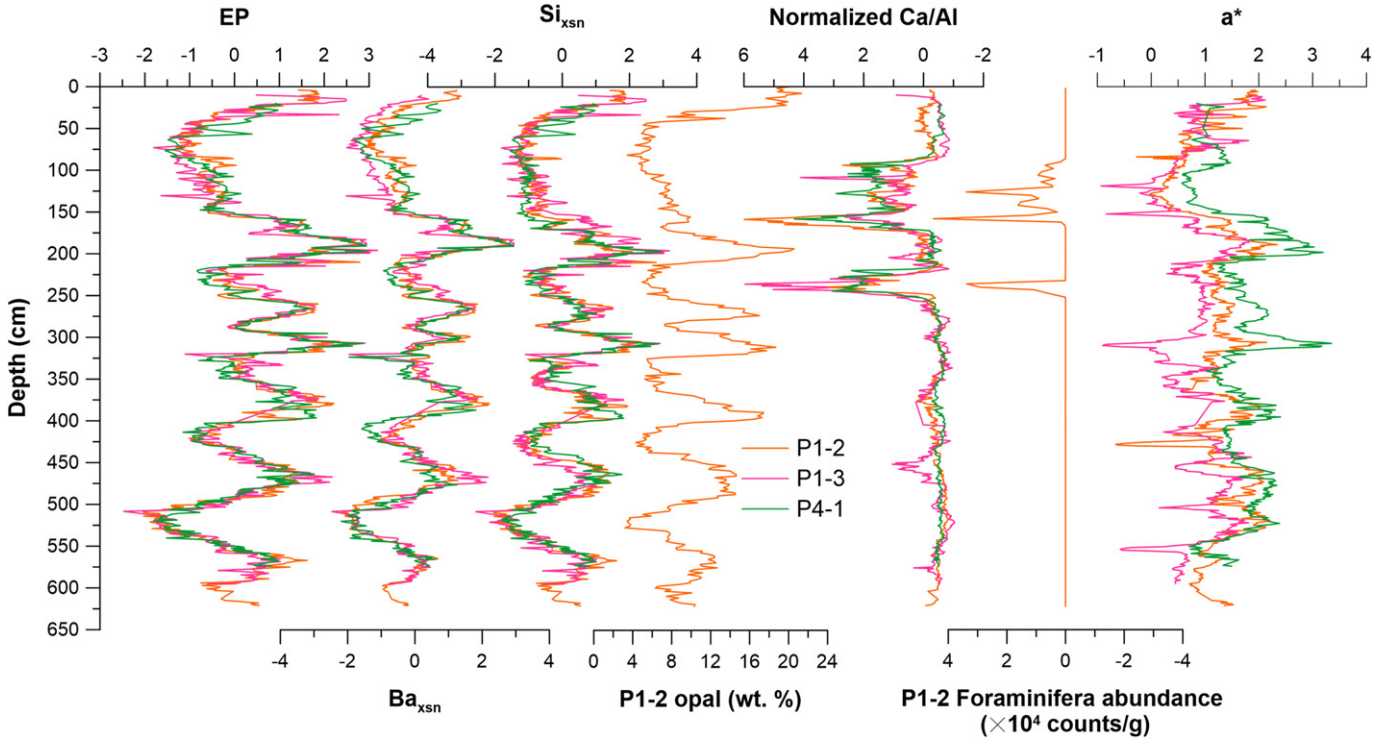

Fig. 4. Distribution patterns of EP, Ba_{xsn}, Si_{xsn}, opal content, normalized Ca/Al and color a* after aligning EPs of P1-3 and P4-1 to that of P1-2.

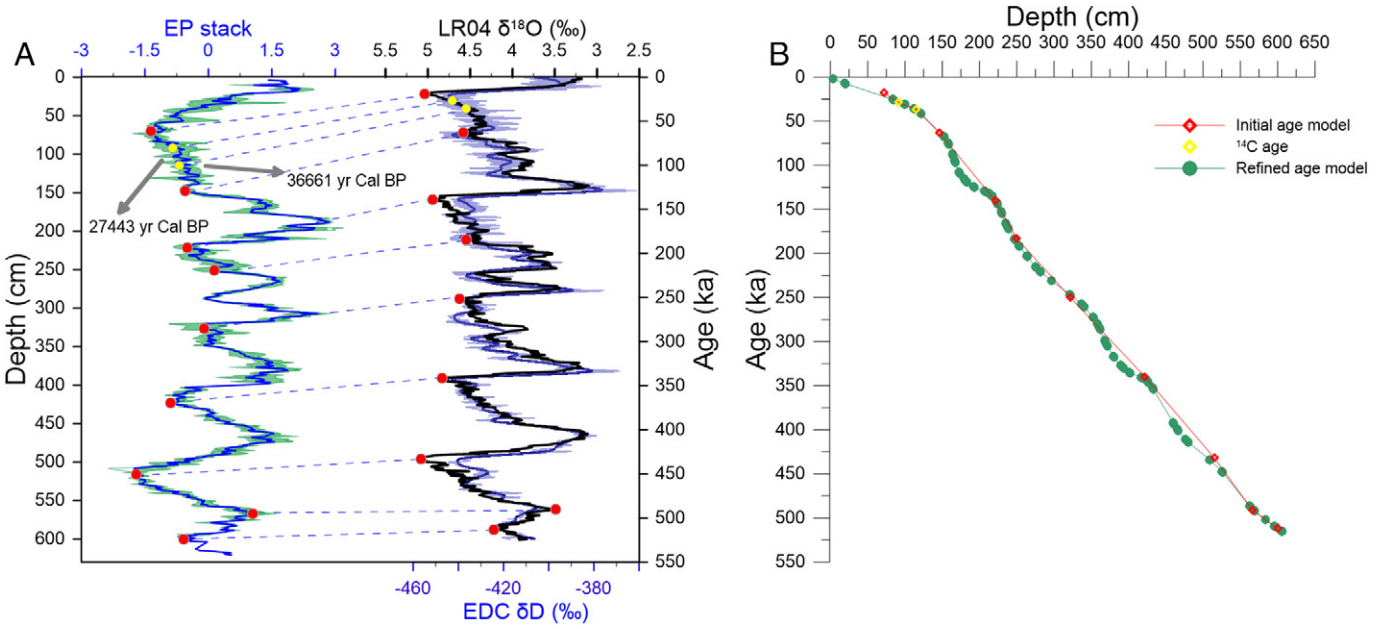

Fig. 5. (A) Preliminary age correlation between the EP stack and LR04-δ^{18}O (Lisiecki and Raymo, 2005). Red dots denote age correlation points between the EP stack and the LR04-δ^{18}O. Two foraminiferal AMS ^{14}C ages are marked as yellow dots. The cyan shade behind the EP stack denotes the variation range of EP for the three cores. The pale blue curve shows the raw EDC-δD (EPICA Community Members, 2004) in EDC3 age model (Parrenin et al., 2007). The deep blue one is the EDC-δD processed with a Fourier low-pass filter of pass-band frequency < 0.1/kyr. (B) Depth-age plots of the controlling points in the initial (red) and final tuned EP stack (green) age models.

Xiao et al., 2016). Predictably, our EP stack also shows a strong similarity to the LR04-δ^{18}O (Lisiecki and Raymo, 2005) and EDC-δD (EPICA Community Members, 2004) records over the last ~520 kyr, although a slight distortion exists in the EP stack likely due to variations in the local sedimentation rate (Fig. 5A). We interpret this similarity as evidence for a climatically controlled export production distribution off Prydz Bay over the studied time interval. Hence, we constructed a preliminary age model by correlating the EP stack to the LR04-δ^{18}O record, assuming there are no obvious phase leads or lags between the local export production variation and global climate change (Fig. 5B). We used the two calibrated AMS ^{14}C ages as first order age constraints and then incorporated other age control points by visually correlating prominent morphological features in the EP stack to their counterparts in the LR04-δ^{18}O stack to produce an initial age model (Fig. 5A).

To improve the matching degree between the initial age model and LR04-δ^{18}O, we employed the match software (Lisiecki and Lisiecki, 2002) and band-pass filters (Paillard et al., 1996) to filter both time series centered at 100-kyr, 41-kyr and 23-kyr, respectively. Then we progressively tuned the EP stack time axis to obtain the best match with the three major orbital cycles in the LR04-δ^{18}O record. The finally tuned age model is shown in Fig. 5B.

In the initial age model, the match degree between the LR04-δ^{18}O record and the EP stack is poor as indicated by the results of filtering analysis (Paillard et al., 1996) and cross wavelet analysis (XWT, Grinsted et al., 2004) (Fig. 6A, B). The determination coefficients (r^2) on the eccentricity (100-kyr), obliquity (41-kyr), and precession (23-kyr) bands (Fig. 6A) and the bulk records (Fig. 6B) between the two time series are 0.618, 0.289, 0.585 and 0.30, respectively. The coherencies between them on the three orbital bands are only occasionally significant and characterized by variable and larger phase angles (Fig. 6B). In the final tuned age model, the match degrees between the two time series are apparently improved (Fig. 6C, D) as indicated by a higher r^2 (Fig 6C, D) and much better coherencies (Fig. 6D) on the three orbital bands.

The final EP stack age model indicates our sediment record off Prydz Bay spans a continuous time period over the last 523 kyrs, with an average sedimentation rate of 1.19 cm/kyr. This sedimentation rate is in good agreement with results from Pleistocene successions at ODP Sites 1167 and 1165 (0.69–1.22 cm/kyr. Theissen et al., 2003; Junttila et al., 2005). Based on the EP tuning approach described above, we constructed age models for cores P1-2, P1-3 and P4-1, respectively (S3). Generally, the EP-based age model of core P1-3 is consistent with the age model constructed by Liu et al. (2015) via Relative Paleo-Intensity (RPI) correlation for the same core (S3). Sedimentary RPI records, however, heavily rely on high sedimentation rates (>10 cm/kyr) to minimize the effect of 'lock-in' depth, which potentially shifts and filters the originally recorded geomagnetic field (Roberts and Winklhofer, 2004). Given the low sedimentation rates in our cores, the temporal resolution and precision of the RPI age model (e.g., Liu et al., 2015) could have been at least partly reduced.

In a recent study on core P1-3, Tang et al. (2016) established an age model using 3 AMS ^{14}C ages on organic matter of bulk sediments plus a few age correlation points visually picked out from comparison between the XRF derived Ba/Ti ratio and LR04-δ^{18}O. In this study, we found some subtle difference of preservation efficiencies between the bio-Si and the bio-Ba (Fig. 3). We suggest the bio-Si increases leading bio-Ba increases during inceptions of deglacial periods was due to better preservation of bio-Si than bio-Ba, while bio-Ba became better preserved after interglacial peaks. Therefore, the inception of each bio-Si rise near every deglacial period was often assigned to preceding late glacial in their age model (Tang et al., 2016), and this needs to be considered if only Ba/Ti ratios were used as time markers.

6.3. Factors affecting regional export production

Solar radiation by altering diatom Fe quotas, can be a key determinant of diatom growth rate at high SO latitudes when silicic acid levels are non-limiting (Boyd et al., 2001; Cheah et al., 2013). Modern diatom blooms in the Prydz Bay region occur immediately after winter sea ice retreat (Pondaven et al., 2000; Pilskaln et al., 2004), indicating that export production is potentially affected by austral spring solar insolation. Past export production as expressed in the EP stack record (Fig. 7A), however, does not match the reconstructed 65°S spring season insolation curve (Laskar et al., 2004) (Fig. 7G). Power spectral

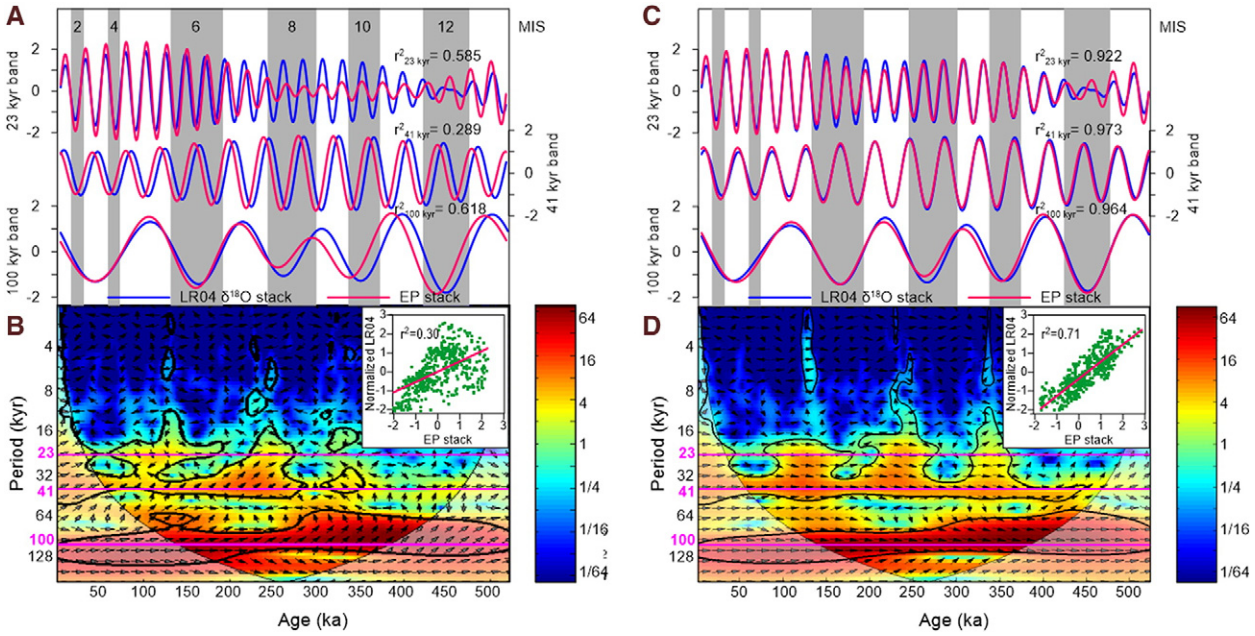

Fig. 6. The coherency variations between the LR04-$\delta^{18}O$ (Lisiecki and Raymo, 2005) and the EP stack-based initial (A, B) and final age models (C, D). (A, C) Fourier band-pass filtered EP stack and LR04-$\delta^{18}O$ on the three major orbital cycles. Determination coefficients (r^2) were calculated on each of the three bands between the EP stack and LR04-$\delta^{18}O$ and were shown on each subplot. Gray shaded stripes indicate the glacial intervals after Lisiecki and Raymo (2005). (B, D) Cross wavelet coherency (XWT) (Grinsted et al., 2004) between the LR04-$\delta^{18}O$ stack and the EP stack in the initial (B) and refined (D) age models. The thick black contour designates the 5% significant level against red noise. The cone of influence (COI), where edge effects might distort the picture, is shown as a lighter shade. Small arrows represent phase deviations between the EP stack and the LR04-$\delta^{18}O$, with upward arrows indicating the EP stack leading the LR04-$\delta^{18}O$, and downward arrows indicating the LR04-$\delta^{18}O$ leading the EP stack. The bold pink lines denote the centers of the three orbital bands. The inset figures are scatter plots of the EP stack vs. the LR04-$\delta^{18}O$.

analysis of the 65°S spring season insolation record shows intensive precessional oscillations, but no eccentricity forcing (Fig. 8A), whereas the EP stack shows a strong power at the eccentricity band and a weak power at the precession band as on the LR04-$\delta^{18}O$ stack (Fig. 8B), indicating variation of the export production is independent of the insolation change.

Sea ice cover potentially can be an important factor limiting solar radiation in high latitude waters (Hillenbrand and Cortese, 2006). In areas with permanent sea ice, export production is almost absent (Frank et al., 1995). In the Seasonal Ice Zone (SIZ), the diatom growing season can be shortened by ice-driven light limitation (Bonn et al., 1998; Presti et al., 2011).

Our core sites are located in today's SIZ. During glacial progressions, the EP stack presents a gradual decline (Fig. 7A), indicating the study area was covered by seasonal sea ice as well. Thus expansion of sea ice during glacial periods may play a role in limiting the local productivity (Presti et al., 2011). However, if nutrients supply to the sea-ice covered region (including our study area) did not reduced, a greater portion of nutrients would remain unused and likely be subjected to Ekman transport northward, subsequently promoting export production in the

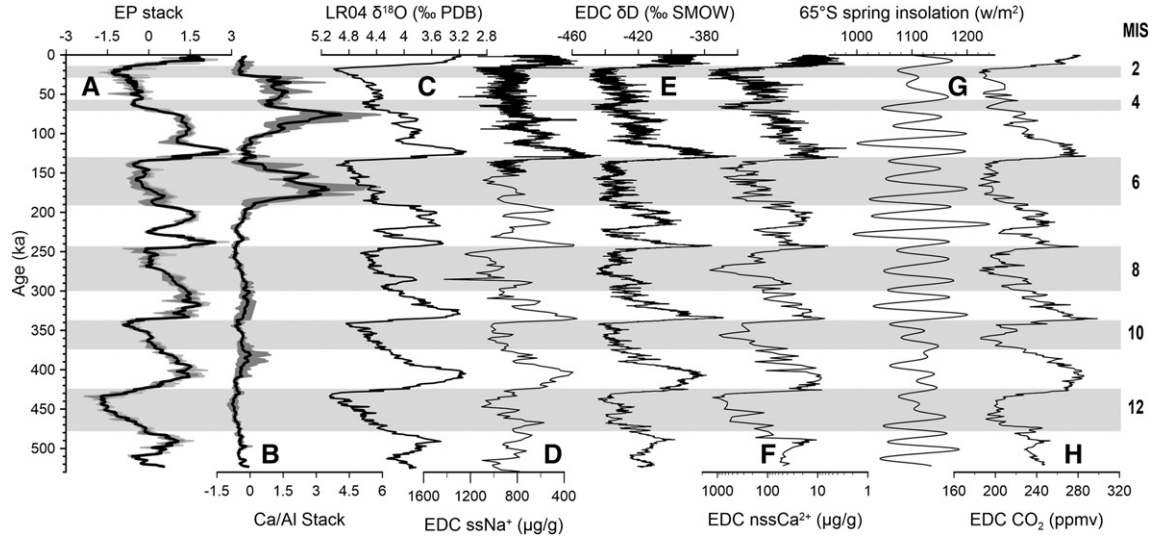

Fig. 7. Temporal variations of (A) EP stack, (B) Ca/Al stack, (C) LR04-$\delta^{18}O$ (Lisiecki and Raymo, 2005), (D) EDC-ssNa$^+$, (E) EDC-δD, (F) EDC-nssCa^{2+}, (G) 65°S spring insolation (Laskar et al., 2004), and (H) EDC-CO_2 over the past ~520 kyr. EDC ice core data are from EPICA-Community-Members (2004). The light-gray shade behind the EP stack in (A) denotes the variation range of the three cores' normalized EP. The Ca/Al stack in (B) is calculated by averaging the normalized Ca/Al ratios for the three cores. The light-gray shade behind the Ca/Al stack in (B) denotes the variation range of the three normalized Ca/Al ratios.

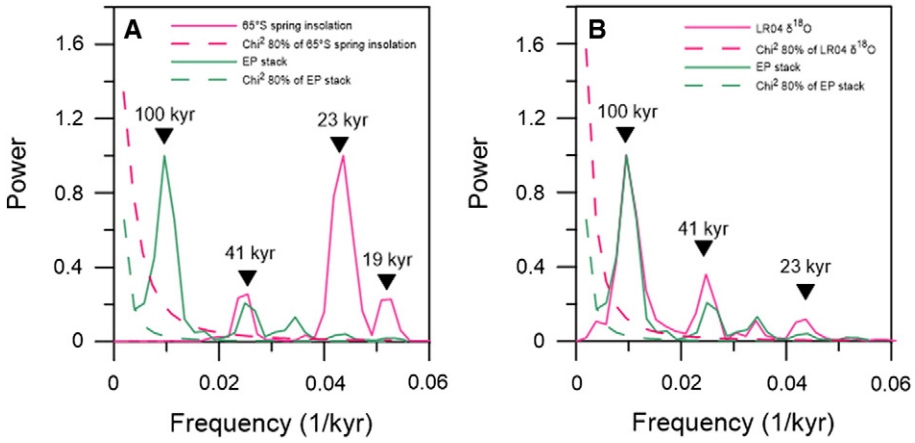

Fig. 8. Comparison of the redfit power spectra (Schulz and Stattegger, 1997) between (A) 65°S spring insolation (Laskar et al., 2004) and EP stack, and (B) between LR04-$\delta^{18}O$ (Lisiecki and Raymo, 2005) and EP stack over the past ~520 kyr. The spectra had been divided by their respective maximum value to facilitate graphical representation.

region where sea ice cover was less extensive or absent. Previous studies on the diatom-bound nitrogen isotope composition throughout the Antarctic Zone (AZ) of the SO (including the Indian sector of SO) indicated nutrient utilization was higher during glacial periods, coincident with lower export production (Robinson and Sigman, 2008; Horn et al., 2011; Studer et al., 2015), suggesting nutrients supply in the SIZ must have been reduced during glacial periods, and hence been an important factor lowering export production in the SIZ, although the role of sea-ice cover cannot be fully ruled out as one cannot expect that the nutrients in the euphotic zone were totally consumed (Sigman et al., 2010).

Thus, we attribute the fluctuation of the EP stack primarily to the combined influence of the variable nutrients supply to the euphotic zone and the seasonal sea ice cover. The anti-phase-like relationship between the EP stack (Fig. 7A) and the EDC-nssCa^{2+} (Fig. 7F) indicates that nutrient-related leverage on the export production was not from dust, but most likely from the ocean water below. The exclusion of a continental sourced nutrient supply is supported by the P1-3 IRD (directly sourced from the continent) record which occurred only in glacial sediments (Liu et al., 2015; Tang et al., 2016). A wind-bound or runoff supply of nutrients, if ever existed, would be mainly confined to the coastal region due to estuarine removal processes (Hodson et al., 2017). Thus the main source of the nutrients supply to the study area must be mainly from the deeper ocean, by vertical mixing or upwelling (Jaccard et al., 2013). Earlier studies demonstrated that wintertime vertical mixing is sensitive to upper ocean density stratification (Robinson and Sigman, 2008; Jaccard et al., 2013), while the strength of upwelling is controlled by the strength and position of Southern Westerly Wind (SWW) and air-sea buoyancy flux (Anderson et al., 2009; Watson and Garabato, 2006; Sigman et al., 2007), both resulting in deep water exposure/ventilation (Watson and Garabato, 2006; Jaccard et al., 2010, 2013). Thus, the coupling between the EP stack and the LR04-$\delta^{18}O$ curve in our study area reflects not only the climate-controlled variation of deep water exposure/ventilation (Tang et al., 2016), but also the influence from the variable extent of seasonal sea ice cover on orbital time scales. Higher levels of the EP stack indicate stronger deep water exposure/ventilation and less seasonal sea ice cover, and vice versa for the low EP levels.

6.4. Implications for atmospheric CO_2

The association between the local export production and carbon cycling is reflected by two aspects. First, export production acting as a 'biological pump' is the major mechanism to extract CO_2 from the atmosphere into the ocean interior (e.g., Jaccard et al., 2005; Sigman et al., 2010). Second, the local export production was regulated by nutrient supply from the ocean interior and seasonal sea ice cover, revealing the combined history of the local deep water exposure/ventilation and extent of sea ice cover. An enhancement in the efficiency of the 'biological pump', a reduction in the rate of deep water exposure/ventilation and an increase in the extent of sea ice cover are all in favor of atmospheric CO_2 drawdown (Watson and Garabato, 2006; Jaccard et al., 2013; Jaccard et al., 2016). Conversely, a reduction in the 'biological pump' efficiency and a less sea ice cover, and an elevation in the rate of deep water exposure/ventilation would promote deeply sequestered CO_2 to outgas (Watson and Garabato, 2006; Jaccard et al., 2013; Jaccard et al., 2016). Thus, the relative efficiency of these processes determines the portioning of CO_2 between the ocean and the atmosphere.

During deglacial periods, the ocean circulation patterns experienced dramatic changes. The volume of abyssal waters of Antarctic origin contracted, and became largely replaced by reactivated, well-ventilated North Atlantic Deep Water (NADW) (Ferrari et al., 2014; Lippold et al., 2016; Sikes et al., 2016). The sharp increases of the EP stack (Fig. 7A) coincide with abrupt rises in atmospheric CO_2 concentration (Fig. 7H) and decrease in sea ice cover (Fig. 7D), indicating enhanced deep water exposure in response to the resumption of overturning circulation (Anderson et al., 2009; Skinner et al., 2010; Horn et al., 2011; Jaccard et al., 2013; Jaccard et al., 2016), which promoted the gas and heat exchange between the ocean and the atmosphere (Sigman and Boyle, 2000; Hillenbrand and Cortese, 2006; Timmermann et al., 2009). Nutrients enriched in the upwelled deep water fueled blooms of the bio-productivity in the euphotic zone, whereas the efficiency of the 'biological pump' decreased as indicated by the nitrogen isotope composition bound within diatoms from the AZ (Horn et al., 2011; Robinson and Sigman, 2008; Studer et al., 2015). The system was thus inadequate to effectively prevent evasion of CO_2 upwelling with the deep water, leading to a transfer of CO_2 to the atmosphere (Jaccard et al., 2016). Meanwhile, the unused nutrients, in particular the dissolved silicon entrained in Antarctic Intermediate Water (AAIW) and Subantarctic Mode Water (SAMW), were transmitted to low latitudes, promoting diatom blooms there (Matsumoto et al., 2002; Hayes et al., 2011; Meckler et al., 2013).

After interglacial peak conditions, atmospheric CO_2 concentrations began to decline (Fig. 7H) along with the reduction in overturning circulation (Brovkin et al., 2007; Hain et al., 2010). The reduced export production (Fig. 7A) suggests the atmospheric CO_2 decline was accompanied by slowdown of the rate of deep water exposure/ventilation and increase in the sea ice cover. Thus, the atmospheric CO_2 decline during these periods might be partly due to increasing sea ice covering, limiting the atmospheric/oceanic CO_2 exchange (e.g., Sigman and Boyle, 2000; Hillenbrand and Cortese, 2006), and partly to the elevated efficiency

of biological pump (Horn et al., 2011; Robinson and Sigman, 2008; Studer et al., 2015), which trumped the rate that CO_2 escaped from the exposed deep water, and subsequently trapped CO_2 into the ocean interior, leading to a decline in the total productivity (Fig. 7A). These mechanisms, however, appear to apply mainly to the early stages of climate cooling (Jaccard et al., 2013), because with the ongoing climate cooling, the rate of deep water exposure would decline to very low levels and sea ice cover would be very extensive, resulting in largely weakening in the rate of air/sea CO_2 exchange in the AZ (Sigman et al., 2010). Numerical modelling suggested only half of the total reduction in atmospheric CO_2 (~40 ppmv) of a glacial cycle occurs during this early stage of climate cooling (Brovkin et al., 2007; Hain et al., 2010).

Concurrent with export production decline in the AZ during the later stages of climate cooling, sediment records north of the APF revealed elevated export production in response to northward shift of the upwelling zone in the SO (Anderson et al., 2014) and enhanced dust-stimulated Fe fertilization (Martínez-Garcia et al., 2009; Martínez-García et al., 2014; Jaccard et al., 2013; Lamy et al., 2014) (Fig. 7F). This elevated export production was characterized by a higher nutrient utilization efficiency (Martínez-García et al., 2014). Consistent with results of numerical simulations (Brovkin et al., 2007; Hain et al., 2010), this higher nutrient utilization efficiency was responsible for further atmospheric CO_2 drawdown (Jaccard et al., 2013; Martínez-Garcia et al., 2009; Martínez-García et al., 2014).

However, the $CaCO_3$ distribution pattern in our study area lacks this typical glacial-interglacial variation mode. Relatively better $CaCO_3$ preservations only occurred within the last two glacial periods (Fig. 7B), i.e. MIS 3-5.4 and MIS 6, indicating the study area only occasionally lying above the lysocline. The absence of $CaCO_3$ accumulation during early glacial-interglacial cycles was also recorded in localities of other Antarctic marginal seas (e.g., Hillenbrand et al., 2009) with reasons remaining unknown. In any case, better $CaCO_3$ preservation in Antarctic marginal seas is common only during glacial periods (e.g., Grobe and Mackensen, 1992; Bonn et al., 1998).

During interglacial periods, high fluxes of organic matter (high export production) promoted CO_2 concentration and enhanced $CaCO_3$ dissolution in the local deep water. During glacial periods, however, the local deep water mass would have a smaller load of dissolved inorganic carbon (DIC) due to low organic matter influx (low export production), thus resulting in better $CaCO_3$ preservations (Bonn et al., 1998).

7. Conclusions

In this paper, we conducted XRF geochemical core scanning, color reflectance measurement, foraminifera abundance counting, AMS ^{14}C dating and biogenic silica measurement on three gravity cores collected from the Prydz deep sea region. Major conclusions were drawn as follows:

(1) A stack of the export production distribution patterns (EP) was constructed by combining the bio-Si and bio-Ba components of the XRF core scanning data, providing a new proxy for the temporal variations of local export production. It presents similar variations to the global climate change pattern recorded in the LR04-$\delta^{18}O$ stack. Further tuning the EP stack to the LR04-$\delta^{18}O$ curve helped to construct age models, showing major orbital cycles as in the LR04-$\delta^{18}O$ record. The final EP stack age model indicates the sediment record spans from the last 523 kyrs, with an average sedimentation rate of 1.19 cm/kyr.

(2) The dominant factors determining the glacial-interglacial pattern of the local export production include the amount of nutrient supply from the ocean deep water and the extent of sea ice cover, while the role of local spring season insolation on the local export production has been minimum. The coupling between the EP stack and the LR04-$\delta^{18}O$ curve reflects climate-controlled variation of deep water exposure/ventilation and the extent of sea ice cover on orbital time scales.

(3) During deglacial periods, sharp increases in export production coincide with abrupt rises in atmospheric CO_2 concentrations, indicating drastic CO_2 outgassing of the exposed deep water in the SO. After interglacial peaks, gradual export production decline is coherent with the decline in atmospheric CO_2 concentrations, suggesting the efficiency of the 'biological pump' to trap CO_2 back into ocean interior trumps the rate that CO_2 escapes from the deep water. However, this mechanism appears to have been operating mainly in the early stages of atmospheric CO_2 drawdown in the AZ. Further atmospheric CO_2 decline would subsequently occur in the SAZ.

Supplementary data to this article can be found online at http://dx.doi.org/10.1016/j.palaeo.2017.06.018.

Acknowledgments

We sincerely thank the editors and the two anonymous reviewers for their critical comments and constructive suggestions which improved the manuscript significantly. This work is part of the project "the 30th Chinese National Antarctic Research Expedition" (CHINARE-2013) financially supported by the Ministry of Finance of China and organized by the Chinese Arctic and Antarctic Administration (CAA) (CHINARE-2012-2020-01-02). We thank the 29th and 30th Chinese Antarctic Expedition cruise members for retrieving the sediments. We specially appreciate Professor Dr. Li Qianyu, who read through the manuscript, carefully revised our expressions and further provided us many precious suggestions.

References

Abelmann, A., Gersonde, R., Cortese, G., Kuhn, G., Smetacek, V., 2006. Extensive phytoplankton blooms in the Atlantic sector of the glacial Southern Ocean. Paleoceanography 21, PA1013. http://dx.doi.org/10.1029/2005PA001199.

Adkins, J.F., McIntyre, K., Schrag, D.P., 2002. The salinity, temperature, and delta O-18 of the glacial deep ocean. Science 298, 1769–1773.

Anderson, R., Kumar, N., Mortlock, R., Froelich, P., Kubik, P., Dittrich-Hannen, B., Suter, M., 1998. Late-Quaternary changes in productivity of the Southern Ocean. J. Mar. Syst. 17, 497–514.

Anderson, R.F., Chase, Z., Fleisher, M.Q., Sachs, J., 2002. The Southern Ocean's biological pump during the last glacial maximum. Deep-Sea Res. II Top. Stud. Oceanogr. 49, 1909–1938.

Anderson, R.F., Ali, S., Bradtmiller, L.I., Nielsen, S.H.H., Fleisher, M.Q., Anderson, B.E., Burckle, L.H., 2009. Wind-driven upwelling in the Southern Ocean and the deglacial rise in atmospheric CO_2. Science 323, 1443–1448.

Anderson, R., Barker, S., Fleisher, M., Gersonde, R., Goldstein, S., Kuhn, G., Mortyn, P., Pahnke, K., Sachs, J., 2014. Biological response to millennial variability of dust and nutrient supply in the Subantarctic South Atlantic Ocean. Philos. Trans. R. Soc. Lond. A 372, 30054.

Archer, D.E., Eshel, G., Winguth, A., Broecker, W., Pierrehumbert, R., Tobis, M., Jacob, R., 2000. Atmospheric pCO_2 sensitivity to the biological pump in the ocean. Glob. Biogeochem. Cycles 14, 1219–1230.

Barbara, L., Crosta, X., Massé, G., Ther, O., 2010. Deglacial environments in eastern Prydz Bay, East Antarctica. Quat. Sci. Rev. 29, 2731–2740.

Bidle, K.D., Manganelli, M., Azam, F., 2002. Regulation of oceanic silicon and carbon preservation by temperature control on bacteria. Science 298, 1980–1984.

Bindoff, N.L., Rosenberg, M.A., Warner, M.J., 2000. On the circulation and water masses over the Antarctic continental slope and rise between 80 and 150°E. Deep-Sea Res. II Top. Stud. Oceanogr. 47, 2299–2326.

Bonn, W.J., Gingele, F.X., Grobe, H., Mackensen, A., Fütterer, D.K., 1998. Palaeoproductivity at the Antarctic continental margin: opal and barium records for the last 400 ka. Palaeogeogr. Palaeoclimatol. Palaeoecol. 139, 195–211.

Boyd, P., Crossley, A., DiTullio, G., Griffiths, F., Hutchins, D., Queguiner, B., Sedwick, P., Trull, T., 2001. Control of phytoplankton growth by iron supply and irradiance in the subantarctic Southern Ocean: experimental results from the SAZ project. J. Geophys. Res. 106 (573-531).

Brovkin, V., Ganopolski, A., Archer, D., Rahmstorf, S., 2007. Lowering of glacial atmospheric CO_2 in response to changes in oceanic circulation and marine biogeochemistry. Paleoceanography 22, PA4202.

Cheah, W., McMinn, A., Griffiths, F.B., Westwood, K.J., Wright, S.W., Clementson, L.A., 2013. Response of phytoplankton photophysiology to varying environmental conditions in the sub-antarctic and polar frontal zone. PLoS One 8, e72165.

Cooper, A.K., O'Brien, P.E., 2004. Leg 188 synthesis: transitions in the glacial history of the Prydz Bay region, East Antarctica, from ODP drilling. Proc. ODP Sci. Results 1–42.

Crosta, X., Pichon, J.J., Burckle, L., 1998a. Application of modern analog technique to marine Antarctic diatoms: reconstruction of maximum sea ice extent at the Last Glacial Maximum. Paleoceanography 13, 284–297.

Crosta, X., Pichon, J.J., Burckle, L.H., 1998b. Reappraisal of Antarctic seasonal sea-ice at the Last Glacial Maximum. Geophys. Res. Lett. 25, 2703–2706.

Crosta, X., Sturm, A., Armand, L., Pichon, J., 2004. Late Quaternary sea ice history in the Indian sector of the Southern Ocean as recorded by diatom assemblages. Mar. Micropaleontol. 50, 209–223.

Domack, W., Jull, T., Donahue, J., 1991. Holocene chronology for the unconsolidated sediments at hole 740A: Prydz Bay, East Antarctica. In: Barron, J., Larsen, B. (Eds.), Proceedings of the Ocean Drilling Program, Scientific Res, pp. 747–750.

Domack, E., Leventer, A., Dunbar, R., Taylor, F., Brachfeld, S., Sjunneskog, C., 2001. Chronology of the Palmer Deep site, Antarctic Peninsula: a Holocene palaeoenvironmental reference for the circum-Antarctic. The Holocene 11, 1–9.

Elderfield, H., Rickaby, R.E.M., 2000. Oceanic Cd/P ratio and nutrient utilization in the glacial Southern Ocean. Nature 405, 305–310.

EPICA-Community-Members, 2004. Eight glacial cycles from an Antarctic ice core. Nature 429, 623–628.

Ferrari, R., Jansen, M.F., Adkins, J.F., Burke, A., Stewart, A.L., Thompson, A.F., 2014. Antarctic sea ice control on ocean circulation in present and glacial climates. Proc. Natl. Acad. Sci. U. S. A. 111, 8753–8758.

Forsberg, C.F., Florindo, F., Grützner, J., Venuti, A., Solheim, A., 2008. Sedimentation and aspects of glacial dynamics from physical properties, mineralogy and magnetic properties at ODP Sites 1166 and 1167, Prydz Bay, Antarctica. Palaeogeogr. Palaeoclimatol. Palaeoecol. 260, 184–201.

Frank, M., Eisenhauer, A., Bonn, W.J., Walter, P., Grobe, H., Kubik, P.W., Dittrich-Hannen, B., Mangini, A., 1995. Sediment redistribution versus paleoproductivity change: Weddell Sea margin sediment stratigraphy and biogenic particle flux of the last 250,000 years deduced from $^{230}Th_{ex}$, ^{10}Be and biogenic barium profiles. Earth Planet. Sci. Lett. 136, 559–573.

Frank, M., Gersonde, R., Rutgers van der Loeff, M., Bohrmann, G., Nürnberg, C.C., Kubik, P., Suter, M., Mangini, A., 2000. Similar glacial and interglacial export bioproductivity in the Atlantic sector of the Southern Ocean: multiproxy evidence and implications for glacial atmospheric CO_2. Paleoceanography 15, 642–658.

Gersonde, R., Crosta, X., Abelmann, A., Armand, L., 2005. Sea-surface temperature and sea ice distribution of the Southern Ocean at the EPILOG Last Glacial Maximum—a circum-Antarctic view based on siliceous microfossil records. Quat. Sci. Rev. 24, 869–896.

Goosse, H., Roche, D.M., Mairesse, A., 2013. Modelling past sea ice changes. Quat. Sci. Rev. 79, 191–206.

Grinsted, A., Moore, J.C., Jevrejeva, S., 2004. Application of the cross wavelet transform and wavelet coherence to geophysical time series. Nonlinear Process. Geophys. 11, 561–566.

Grobe, H., Mackensen, A., 1992. Late Quaternary climatic cycles as recorded in sediments from the Antarctic continental margin. The Antarctic Paleoenvironment: A Perspective on Global Change: Part One, pp. 349–376.

Hain, M.P., Sigman, D.M., Haug, G.H., 2010. Carbon dioxide effects of Antarctic stratification, North Atlantic intermediate water formation, and subantarctic nutrient drawdown during the last ice age: diagnosis and synthesis in a geochemical box model. Glob. Biogeochem. Cycles 24.

Hannah, M.J., 2006. The palynology of ODP site 1165, Prydz Bay, East Antarctica: a record of Miocene glacial advance and retreat. Palaeogeogr. Palaeoclimatol. Palaeoecol. 231, 120–133.

Hayes, C.T., Anderson, R.F., Fleisher, M.Q., 2011. Opal accumulation rates in the equatorial Pacific and mechanisms of deglaciation. Paleoceanography 26.

Hillenbrand, C.D., Cortese, G., 2006. Polar stratification: a critical view from the Southern Ocean. Palaeogeogr. Palaeoclimatol. Palaeoecol. 242, 240–252.

Hillenbrand, C.D., Grobe, H., Diekmann, B., Kuhn, G., Fütterer, D.K., 2003. Distribution of clay minerals and proxies for productivity in surface sediments of the Bellingshausen and Amundsen seas (West Antarctica)–relation to modern environmental conditions. Mar. Geol. 193, 253–271.

Hillenbrand, C.D., Kuhn, G., Frederichs, T., 2009. Record of a Mid-Pleistocene depositional anomaly in West Antarctic continental margin sediments: an indicator for ice-sheet collapse? Quat. Sci. Rev. 28, 1147–1159.

Hodson, A., Nowak, A., Sabacka, M., Jungblut, A., Navarro, F., Pearce, D., Ávila-Jiménez, M.L., Convey, P., Vieira, G., 2017. Climatically sensitive transfer of iron to maritime Antarctic ecosystems by surface runoff. Nat. Commun. 8, 14499.

Horn, M.G., Beucher, C.P., Robinson, R.S., Brzezinski, M.A., 2011. Southern ocean nitrogen and silicon dynamics during the last deglaciation. Earth Planet. Sci. Lett. 310, 334–339.

Jaccard, S.L., Galbraith, E.D., 2012. Large climate-driven changes of oceanic oxygen concentrations during the last deglaciation. Nat. Geosci. 5, 151–156.

Jaccard, S.L., Haug, G.H., Sigman, D.M., Pedersen, T.F., Thierstein, H.R., Rohl, U., 2005. Glacial/interglacial changes in subarctic North Pacific stratification. Science 308, 1003–1006.

Jaccard, S., Galbraith, E., Sigman, D., Haug, G., 2010. A pervasive link between Antarctic ice core and subarctic Pacific sediment records over the past 800 kyrs. Quat. Sci. Rev. 29, 206–212.

Jaccard, S., Hayes, C.T., Martínez-García, A., Hodell, D., Anderson, R.F., Sigman, D., Haug, G., 2013. Two modes of change in Southern Ocean productivity over the past million years. Science 339, 1419–1423.

Jaccard, S.L., Galbraith, E.D., Martínez-García, A., Anderson, R.F., 2016. Covariation of deep Southern Ocean oxygenation and atmospheric CO_2 through the last ice age. Nature 530, 207–210.

Jansen, J., Van der Gaast, S., Koster, B., Vaars, A., 1998. CORTEX, a shipboard XRF-scanner for element analyses in split sediment cores. Mar. Geol. 151, 143–153.

Junttila, J., Ruikka, M., Strand, K., 2005. Clay-mineral assemblages in high-resolution Plio-Pleistocene interval at ODP site 1165, Prydz Bay, Antarctica. Glob. Planet. Chang. 45, 151–163.

Kumar, N., Anderson, R., Mortlock, R., Froelich, P., Kubik, P., Dittrich-Hannen, B., Suter, M., 1995. Increased biological productivity and export production in the glacial Southern Ocean. Nature 378, 675–680.

Lamy, F., Gersonde, R., Winckler, G., Esper, O., Jaeschke, A., Kuhn, G., Ullermann, J., Martinez-Garcia, A., Lambert, F., Kilian, R., 2014. Increased dust deposition in the Pacific Southern Ocean during glacial periods. Science 343, 403–407.

Laskar, J., Robutel, P., Joutel, F., Gastineau, M., Correia, A., Levrard, B., 2004. A long-term numerical solution for the insolation quantities of the Earth. Astron. Astrophys. 428, 261–285.

Lippold, J., Gutjahr, M., Blaser, P., Christner, E., de Carvalho Ferreira, M.L., Mulitza, S., Christl, M., Wombacher, F., Böhm, E., Antz, B., Cartapanis, O., Vogel, H., Jaccard, S.L., 2016. Deep water provenance and dynamics of the (de)glacial Atlantic meridional overturning circulation. Earth Planet. Sci. Lett. 445, 68–78.

Lisiecki, L.E., Lisiecki, P.A., 2002. Application of dynamic programming to the correlation of paleoclimate records. Paleoceanography 17, 1–12.

Lisiecki, L.E., Raymo, M.E., 2005. A Pliocene-Pleistocene stack of 57 globally distributed benthic $\delta^{18}O$ records. Paleoceanography 20, 1–17.

Liu, Helin, Chen, Zhihua, Ge, Shulan, Xiao, Wenshen, Wang, Haozhuang, Tang, Zheng, Huang, Yuanhui, Zhao, Renjie, Wu, Li, 2015. Late quaternary sedimentary records and paleoceanographic implications from the core on continental slope off the Prydz Bay, East Antarctic. Mar. Geol. Quat. Geol. 33 (3), 209–217.

Luthi, D., Le Floch, M., Bereiter, B., Blunier, T., Barnola, J.-M., Siegenthaler, U., Raynaud, D., Jouzel, J., Fischer, H., Kawamura, K., Stocker, T.F., 2008. High-resolution carbon dioxide concentration record 650,000–800,000 years before present. Nature 453, 379–382.

Manoj, M., Thamban, M., 2015. Shifting frontal regimes and its influence on bioproductivity variations during the Late Quaternary in the Indian sector of Southern Ocean. Deep-Sea Res. II Top. Stud. Oceanogr. 118, 261–274.

Marshall, J., Speer, K., 2012. Closure of the meridional overturning circulation through Southern Ocean upwelling. Nat. Geosci. 5, 171–180.

Martínez-Garcia, A., Rosell-Melé, A., Geibert, W., Gersonde, R., Masqué, P., Gaspari, V., Barbante, C., 2009. Links between iron supply, marine productivity, sea surface temperature, and CO_2 over the last 1.1 Ma. Paleoceanography 24, 432–451.

Martínez-García, A., Sigman, D.M., Ren, H., Anderson, R.F., Straub, M., Hodell, D.A., Jaccard, S.L., Eglinton, T.I., Haug, G.H., 2014. Iron fertilization of the Subantarctic Ocean during the last ice age. Science 343, 1347–1350.

Matsumoto, K., Sarmiento, J.L., Brzezinski, M.A., 2002. Silicic acid leakage from the Southern Ocean: a possible explanation for glacial atmospheric pCO_2. Glob. Biogeochem. Cycles 16.

McManus, J., Berelson, W.M., Klinkhammer, G.P., Johnson, K.S., Coale, K.H., Anderson, R.F., Kumar, N., Burdige, D.J., Hammond, D.E., Brumsack, H.J., 1998. Geochemistry of barium in marine sediments: implications for its use as a paleoproxy. Geochim. Cosmochim. Acta 62, 3453–3473.

Meckler, A., Sigman, D., Gibson, K., François, R., Martínez-García, A., Jaccard, S., Röhl, U., Peterson, L., Tiedemann, R., Haug, G., 2013. Deglacial pulses of deep-ocean silicate into the subtropical North Atlantic Ocean. Nature 495, 495–498.

Moore, J.K., Abbott, M.R., Richman, J.G., Nelson, D.M., 2000. The Southern Ocean at the last glacial maximum: a strong sink for atmospheric carbon dioxide. Glob. Biogeochem. Cycles 14, 455–475.

Mortlock, R.A., Froelich, P.N., 1989. A simple method for the rapid determination of biogenic opal in pelagic marine sediments. Deep Sea Res. Part A 36, 1415–1426.

Paillard, D., Labeyrie, L., Yiou, P., 1996. Macintosh program performs time-series analysis. Eos. Trans. AGU 77, 379.

Parrenin, F., Barnola, J.-M., Beer, J., Blunier, T., Castellano, E., Chappellaz, J., Dreyfus, G., Fischer, H., Fujita, S., Jouzel, J., 2007. The EDC3 chronology for the EPICA dome C ice core. Clim. Past 3, 485–497.

Passchier, S., O'Brien, P., Damuth, J., Januszczak, N., Handwerger, D., Whitehead, J., 2003. Pliocene–Pleistocene glaciomarine sedimentation in eastern Prydz Bay and development of the Prydz trough-mouth fan, ODP sites 1166 and 1167, East Antarctica. Mar. Geol. 199, 279–305.

Paytan, A., Griffith, E.M., 2007. Marine barite: recorder of variations in ocean export productivity. Deep-Sea Res. II Top. Stud. Oceanogr. 54, 687–705.

Pilskaln, C.H., Manganini, S.J., Trull, T.W., Armand, L., Howard, W., Asper, V.L., Massom, R., 2004. Geochemical particle fluxes in the Southern Indian Ocean seasonal ice zone: Prydz Bay region, East Antarctica. Deep-Sea Res. I Oceanogr. Res. Pap. 51, 307–332.

Pondaven, P., Ragueneau, O., Treguer, P., Hauvespre, A., Dezileau, L., Reyss, J.L., 2000. Resolving the 'opal paradox' in the Southern Ocean. Nature 405, 168–172.

Presti, M., Barbara, L., Denis, D., 2011. Sediment delivery and depositional patterns off Adélie Land (East Antarctica) in relation to late Quaternary climatic cycles. Mar. Geol. 284, 96–113.

Pugh, R.S., McCave, I.N., Hillenbrand, C.D., Kuhn, G., 2009. Circum-Antarctic age modelling of Quaternary marine cores under the Antarctic Circumpolar Current: ice-core dust–magnetic correlation. Earth Planet. Sci. Lett. 284, 113–123.

Reimer, P.J., Bard, E., Bayliss, A., Beck, J.W., Blackwell, P.G., Bronk Ramsey, C., Buck, C.E., Cheng, H., Edwards, R.L., Friedrich, M., 2013. IntCal13 and Marine 13 radiocarbon age calibration curves 0–50,000 years cal BP. Radiocarbon 55, 1869–1887.

Roberts, A.P., Winklhofer, M., 2004. Why are geomagnetic excursions not always recorded in sediments? Constraints from post-depositional remanent magnetization lock-in modelling. Earth Planet. Sci. Lett. 227, 345–359.

Robinson, R.S., Sigman, D.M., 2008. Nitrogen isotopic evidence for a poleward decrease in surface nitrate within the ice age Antarctic. Quat. Sci. Rev. 27, 1076–1090.

Röthlisberger, R., Crosta, X., Abram, N.J., Armand, L., Wolff, E.W., 2010. Potential and limitations of marine and ice core sea ice proxies: an example from the Indian Ocean sector. Quat. Sci. Rev. 29, 296–302.

Sayles, F., Martin, W., Chase, Z., Anderson, R., 2001. Benthic remineralization and burial of biogenic SiO_2, $CaCO_3$, organic carbon, and detrital material in the Southern Ocean along a transect at 170° West. Deep-Sea Res. II Top. Stud. Oceanogr. 48, 4323–4383.

Schenau, S., Prins, M., De Lange, G., Monnin, C., 2001. Barium accumulation in the Arabian Sea: controls on barite preservation in marine sediments. Geochim. Cosmochim. Acta 65, 1545–1556.

Schneider-Mor, A., Yam, R., Bianchi, C., Kunz-Pirrung, M., Gersonde, R., Shemesh, A., 2005. Diatom stable isotopes, sea ice presence and sea surface temperature records of the past 640 ka in the Atlantic sector of the Southern Ocean. Geophys. Res. Lett. 32, L10704. http://dx.doi.org/10.1029/2005GL022543.

Schulz, M., Stattegger, K., 1997. SPECTRUM: spectral analysis of unevenly spaced paleoclimatic time series. Comput. Geosci. 23, 929–945.

Sigman, D.M., Boyle, E.A., 2000. Glacial/interglacial variations in atmospheric carbon dioxide. Nature 407, 859–869.

Sigman, D.M., de Boer, A.M., Haug, G.H., 2007. In: Schmittner, A., Chiang, J.C.H., Hemming, S.R. (Eds.), Ocean Circulation: Mechanisms and Impacts. American Geophysical Union, Washington, DC, pp. 335–349.

Sigman, D.M., Hain, M.P., Haug, G.H., 2010. The polar ocean and glacial cycles in atmospheric CO_2 concentration. Nature 466, 47–55.

Sikes, E., 2012. Radiocarbon in Deep Water in the Southwest Pacific and Southern Ocean since the Last Glacial Maximum. Quat. Int. 279-280, 450.

Sikes, E.L., Elmore, A.C., Allen, K.A., Cook, M.S., Guilderson, T.P., 2016. Glacial water mass structure and rapid delta O-18 and delta C-13 changes during the last glacial termination in the Southwest Pacific. Earth Planet. Sci. Lett. 456, 87–97.

Skinner, L.C., Fallon, S., Waelbroeck, C., Michel, E., Barker, S., 2010. Ventilation of the Deep Southern Ocean and Deglacial CO_2 rise. Science 328, 1147–1151.

Stephens, B.B., Keeling, R.F., 2000. The influence of Antarctic sea ice on glacial–interglacial CO_2 variations. Nature 404, 171–174.

Studer, A.S., Sigman, D.M., Martinez-Garcia, A., Benz, V., Winckler, G., Kuhn, G., Esper, O., Lamy, F., Jaccard, S.L., Wacker, L., Oleynik, S., Gersonde, R., Haug, G.H., 2015. Antarctic zone nutrient conditions during the last two glacial cycles. Paleoceanography 30, 845–862.

Stuiver, M., Reimer, J., 1993. Extended ^{14}C data base and revised CALIB 3.0 ^{14}C age calibration program. Editorial Comment. 35, pp. 215–230.

Tang, Z., Shi, X., Zhang, X., Chen, Z., Chen, M.-T., Wang, X., Wang, H., Liu, H., Lohmann, G., Li, P., Ge, S., Huang, Y., 2016. Deglacial biogenic opal peaks revealing enhanced Southern Ocean upwelling during the last 513 ka. Quat. Int. 425, 445–452.

Taylor, F., McMinn, A., 2002. Late quaternary diatom assemblages from Prydz Bay, Eastern Antarctica. Quat. Res. 57, 151–161.

Theissen, K.M., Dunbar, R.B., Cooper, A.K., Mucciarone, D.A., Hoffmann, D., 2003. The Pleistocene evolution of the East Antarctic Ice Sheet in the Prydz bay region: stable isotopic evidence from ODP site 1167. Glob. Planet. Chang. 39, 227–256.

Tian, J., Xie, X., Ma, W., Jin, H., Wang, P., 2011. X-ray fluorescence core scanning records of chemical weathering and monsoon evolution over the past 5 Myr in the southern South China Sea. Paleoceanography 26, 1–17.

Timmermann, A., Timm, O., Stott, L., Menviel, L., 2009. The roles of CO_2 and orbital forcing in driving southern hemispheric temperature variations during the last 21 000 yr. J. Clim. 22, 1626–1640.

Tjallingii, R., Röhl, U., Kölling, M., Bickert, T., 2007. Influence of the water content on X-ray fluorescence core-scanning measurements in soft marine sediments. Geochem. Geophys. Geosyst. 8, 323–345.

Toggweiler, J.R., Russell, J.L., Carson, S.R., 2006. Midlatitude westerlies, atmospheric CO_2, and climate change during the ice ages. Paleoceanography 21 (2), 1–15.

Tribovillard, N., Algeo, T.J., Lyons, T., Riboulleau, A., 2006. Trace metals as paleoredox and paleoproductivity proxies: an update. Chem. Geol. 232, 12–32.

van Beek, P., Reyss, J.L., Bonte, P., Schmidt, S., 2003. Sr/Ba in barite: a proxy of barite preservation in marine sediments? Mar. Geol. 199, 205–220.

Vaz, R.A.N., Lennon, G.W., 1996. Physical oceanography of the Prydz Bay region of Antarctic waters. Deep-Sea Res. I Oceanogr. Res. Pap. 43, 603–641.

Watson, A.J., Garabato, A.C.N., 2006. The role of Southern Ocean mixing and upwelling in glacial-interglacial atmospheric CO_2 change. Tellus Ser. B Chem. Phys. Meteorol. 58, 73–87.

Weber, M.E., Kuhn, G., Sprenk, D., Rolf, C., Ohlwein, C., Ricken, W., 2012. Dust transport from Patagonia to Antarctica - a new stratigraphic approach from the Scotia Sea and its implications for the last glacial cycle. Quat. Sci. Rev. 36, 177–188.

Weltje, G.J., Tjallingii, R., 2008. Calibration of XRF core scanners for quantitative geochemical logging of sediment cores: theory and application. Earth Planet. Sci. Lett. 274, 423–438.

Xiao, W., Frederichs, T., Gersonde, R., Kuhn, G., Esper, O., Zhang, X., 2016. Constraining the dating of late Quaternary marine sediment records from the Scotia Sea (Southern Ocean). Quat. Geochronol. 31, 97–118.

Yabuki, T., Suga, T., Hanawa, K., Matsuoka, K., Kiwada, H., Watanabe, T., 2006. Possible source of the antarctic bottom water in the Prydz Bay region. J. Oceanogr. 62, 649–655.